NanoScience Technology, Volume 12 (2024), pp: 1-25

NanoScience Technology

Journal homepage : https://jnanoscitec.com

A Review on Modeling and Simulation of COF-Based Lithium-ion Batteries

A. Jabbarinick [a], A. Houmani [a], Z. Harati Zaveh [a], B. Abyaz [a], A. Ghafari [a,c], B. Dashtipour [a], M. Sam [a,b], F. Asgari Sima [a], S. Akbari [a,b,c *]

[a] *NanoSciTec GmbH, Hermann Weinhauser str. 67, Munich, 81867, Germany*
[b] *Green International World Ltd, 128 City Road, London, United Kingdom*
[c] *BioMwdEx GmbH, weyringerg 37 Stiege 1, 1040, Wein, Austria*

Abstract

Lithium-ion batteries (LIBs) serve as widespread energy storage solutions in portable electronics, electric vehicles, and renewable energy systems due to their high energy density and rechargeability. Covalent organic frameworks (COFs) exhibit promising potential in LIBs, contributing to enhanced battery performance through improved conductivity, stability, and capacity retention, thus paving the way for more efficient and sustainable energy storage technologies. The advantages of theoretical modeling and simulation methods in COF-based LIBs research are discussed in this contribution. From finite element analysis (FEA) for mechanical perspectives to density functional theory (DFT) for electronic structure considerations and computational fluid dynamics (CFD) for electrolyte and thermal behavior simulations, this study showcases the diverse toolkit used. Electrochemical impedance spectroscopy (EIS) modeling and the integration of machine learning (ML) approaches further enrich the understanding of electrochemical processes and data analysis within lithium batteries. Specific attention is given to modeling and simulating COF-based anodes, cathodes, electrolytes, and separators. This review sheds light on the potential of COFs in revolutionizing lithium battery technology and the importance of computational approaches in advancing their development.

Keywords: *Lithium-ion batteries, Covalent organic frameworks, Battery modeling and simulation, Density functional theory, Machine learning*

© Article info: Accepted by: 11 January 2024, Published by: 26 January 2024.

Table of Contents

* Corresponding author: S. Akbari. Tel.: +49-151-664-32106 E-mail address: somayeh.akbari@nanoscitec.com

1. Introduction

Non-renewable energies are nearing exhaustion, prompting a shift in energy utilization to lower carbon emanations due to rising vitality requests [1, 2]. In recent decades, electronic innovation advancements have led to a significant rise in electric vehicles and convenient gadget utilization. Electrochemical energy storage systems offer cost-effectiveness, durability, and environmental safety, making them versatile for diverse energy needs. From a historical standpoint, LIBs with high energy density and a high discharge voltage (3.7 V) were first developed in Japan and released in 1991 [3]. LIBs offer an attractive alternative to the long-standing lead-acid batteries (LABs) dominating the rechargeable battery industry for more than a century. Despite their widespread acceptance and safety, LABs exhibit drawbacks such as low energy density (typically 30 to 40 $Wh\,kg^{-1}$) and limited cycle endurance (usually fewer than 500 deep cycles) [4, 5]. Extensive research in the past three decades has yielded significant advancements in LIB technology, leading to enhanced durability and reduced life cycle expenses [6, 7].

While alkaline nickel-cadmium batteries boast extended lifespans and resilience against overcharging and over discharging, their drawbacks, including the memory effect caused by improper charging and the release of toxic cadmium into the environment at the battery's end-of-life, overshadow these benefits [8]. On the other hand, LIBs are smaller in volume and weight than cadmium batteries, which makes them popular among rechargeable batteries. Metal-based inorganic compounds containing cobalt, iron, or manganese serve as electrodes in LIBs, altering the metal's charge and maintaining battery stability through specific counter-ions within their crystal structures. However, relying solely on specific counter-ions limits adaptability to various alkali metals and involves environmentally harmful extraction methods, restricting widespread battery applicability. Conversely, organic materials emerge as promising options for enhancing energy storage systems (ESSs) due to their flexibility, abundant availability, and cost-effectiveness. Their adaptable structures can be tailored using diverse methods, allowing customization of properties such as conductivity, capacity, and shape. This versatility enables the use of one organic material across different battery types, like

lithium-ion and sodium-ion, without exact substance compatibility constraints [9].

The first type of porous materials made using reticular chemistry are called metal-organic frameworks (MOF). These materials have frameworks made by connecting clusters with strong covalent bonds [10]. In 2005, Yaghi and his team demonstrated the practical utilization of topological principles to create porous covalent organic frameworks (COFs). These structures, formed by covalent bonds, exhibit a network structure in two or three dimensions, featuring pore sizes spanning 7 to 27 angstroms [11]. COFs have more orderly holes than regular MOF materials and increased thermodynamic steadiness [12]. Due to their skeletal structure, COFs possess added functionalities to achieve specific attributes. With their lightweight constituents bonded covalently, COFs showcase low mass densities, remarkable thermal stability (up to 500℃ to 60℃), sustained porosity, and high surface areas (ranging from 711 to 1590 square meters per gram) [13]. COFs serve as purpose-built porous substances, offering a versatile platform across various applications such as gas adsorption, semiconductor behavior, heterogeneous catalysis, and improving battery performance [14, 15]. COFs offer distinct attributes enhancing electrode performance, like robust chemical and thermal stability alongside porous functional structures. Their crucial role spans electrode-cathode, electrolyte, and separator components within lithium batteries, contributing significantly to their function [16, 17].

The challenge of boosting energy density in LIBs arises from the higher capacities of anodes relative to cathodes. Positive electrodes usually have specific capacities ranging between 150–20 $mAh\ g^{-1}$, ultimately determining the battery's overall capacity in the lithium-ion system [18, 19]. These capacities are limited by the rate of lithium intercalation into the metal oxides. Additionally, with regular use, conventional LIBs lose essential capacity and need to be replaced often [20, 21]. The cathode is the positive electrode, where reduction (gain of electrons) occurs, and using COF cathode materials, concentrate on creating carbonyl structures with distinct links that separate into two generations. The first generation's cathode materials have boronate [22] and boroxine [23] linkages, which are unstable and cannot prevent the dissolution of COFs in electrolytes. And the second generation of COF cathode materials has imine and ketone [24] stable linkages, which can significantly increase electrolyte recycling stability regardless of difficult synthesis conditions [25, 26]. Overall, COF materials exhibit excellent stability, are easily functionalizable, and have open channels, indicating their potential utility as a cathode material in reversible lithium batteries [27].

Increased distortion and localized breakdown of the Co-N coordination bonds, which increase accessibility to the Li-ion intercalation sites, are thought to be the causes of the cycling-induced improvement in the COF anode's performance. Overall, because of their stable structures, tunable pore diameters, and enhanced lithium storage ability, imide-based COFs hold potential as anode materials for LIBs [28, 29].

COFs feature a well-structured framework and channels that allow ions to travel freely. Adding ionic characteristics to COF frameworks makes them a suitable candidate for solid electrolytes, particularly for transporting lithium ions [30]. COFs may be superior to polymer-based electrolytes for lithium ions due to their ease of functionality. They perform effectively at extreme temperatures, even up to 100℃ [31]. COFs feature narrow channels that allow ions to travel fast. These new materials, known as COF-IL, are able to endure extremely high temperatures of up to 400°C. Furthermore, these electrolyte combinations have a remarkable capacity to conduct Li^{+}ions, with values reaching as high as 2.60×10^{-3}S/cm at 120℃. This is one of the highest levels ever seen among doped porous organic materials [32].

As a thin barrier that keeps the anode and cathode from coming into direct contact, the separator is a crucial component of a cell [33]. Its particular structure, which comes from COF, gives ions specific permeability. This structural advantage, independent of operating temperature (25°C or 55°C), leads to significant electrochemical benefits in lithium transition metal oxide cathode-based batteries, including extended cycle endurance and improved rate performance [34]. In lithium cells, the COF-coated polymer separator showed a noticeably higher Li^{+} transfer number of 0.76 in comparison to the limited Li^{+} transfer number of 0.38 displayed by the standard polymer separator. Ion transfer is facilitated by the high, consistent

porosity and maintains the consistent current density seen in COFs [35].

The integration of COFs into LIBs depends on a combined approach of tests and modeling. The use of COFs in LIBs needs a thorough understanding of their structural dynamics, ion transport processes, and electrochemical behaviors, which are sometimes sophisticated and difficult to explain purely by experimental techniques [36, 37].

Modeling and simulation play a vital role in speeding up understanding, forecasting, and advancement in this field. Investigate depends on modeling to explore COF structures at atomic levels, anticipate their properties, and get complex ion diffusion pathways. Recreations help in assessing COF performance under various conditions, which is vital for designing and optimizing COF-based battery frameworks. Several methods and methodologies are used in simulation and modeling. Among the notable tools and methodologies are:

Finite Element Analysis (FEA) to demonstrate the basic and mechanical perspectives of battery components [38, 39].

Density Functional Theory (DFT) to consider the electronic structure of materials, giving bits of knowledge into the properties of anode materials and their intelligence with lithium particles [40, 41].

Computational Fluid Dynamics (CFD) it helps imitate how electrolytes move and how heat moves in the battery [42, 43].

Electrochemical Impedance Spectroscopy (EIS) modeling is used to understand the electrochemical forms inside batteries, counting resistance, capacitance, and charge exchange energy [44].

Simulation platforms and software such as ANSYS Fluent and COMSOL Multiphysics offer capabilities for battery modeling and recreations, each centering on particular perspectives like electrochemistry, thermal behavior, or basic examination [45-47].

Also, machine learning (ML) is becoming more significant in the simulation and modeling of LIBs. Large datasets created from experimental investigations, simulations, or even monitoring real-world battery performance are analyzed using ML approaches [48, 49].

Delving into theoretical modeling and simulation methods, this review aims to delineate the underlying principles and scope of employing these tools. Furthermore, this article embarks on an expedition through computational methods and modeling techniques specifically tailored to simulate COF-based lithium batteries. It delineates their key performance metrics and dissects the modeling intricacies of COF-based anodes, cathodes, electrolytes, and separators. By amalgamating theoretical insights with practical applications, this review aspires to furnish a comprehensive understanding, shedding light on the promising prospects and potential advancements in COF-enabled lithium battery technology.

2. Modelling and simulation of lithium-ion batteries

There are various classifications for simulating LIBs, with the most significant and comprehensive being the classification based on the size of the model under study. This section explores these simulations and how they fit into each specific category. When simulating LIBs, one key factor to consider is the size of the model being studied, which can refer to both the physical dimensions of the battery and the scale and complexity of the simulation itself. Simulations can be classified based on the scale of the model, ranging from the atomic and molecular level to the macroscopic level. At the atomic and molecular level, simulations focus on understanding the fundamental processes and behaviors of the materials and components within the battery, such as the movement of lithium ions, electron transfer, and chemical reactions. Moving up in scale, mesoscale simulations consider the interactions and behaviors of individual components within the battery, such as the electrodes, electrolyte, and interfaces. These simulations provide insight into the performance and degradation mechanisms at a more detailed level than macroscopic models.

Finally, macroscopic simulations encompass the entire battery system and its behavior as a whole. These simulations are often used to predict overall performance, such as capacity, voltage, and aging, and are valuable for understanding the battery's behavior in real-world applications. Each of these classifications

offers unique insights into the behavior and performance of LIBs. Understanding how they fit into each specific category can help researchers and engineers choose the most appropriate simulation approach for their specific needs.

2.1 Molecular models

2.1.1 Density Functional Theory (DFT)

DFT is a computational approach that focuses on the electronic structure of materials, guided by Hohenberg and Kohn's theorems, which link a system's properties solely to electron density. Widely used in battery research, DFT allows for the exploration and prediction of battery dynamics, including voltage [50, 51], capacity [52], diffusion [53], and electrode degradation [54]. It is instrumental in designing optimized battery components, manipulating electrodes through doping [55] or coating [56], and refining the solid electrolyte interphase (SEI) layer to enhance performance [57]. A number of DFT applications can be seen in Figure 1.

DFT operates on the principle that the ground state energy and various properties of a system can be derived through functionals of the electron density, a function dependent solely on spatial coordinates. However, the exact structure of the energy functional remains unknown and requires approximation through certain assumptions and empirical parameters. The effectiveness and precision of DFT depend on the selection of these approximations and the basis set used in calculations. DFT is based on the concept that the electron density, representing the normalized N-electron wave function, is a fundamental characteristic rather than numerous many-body wave functions. This significantly accelerates calculations, as the electron density depends on just three (x, y, z) variables, whereas many-body electron wave functions (involving N atoms) depend on 3N variables. Equation (1) represents Schrödinger's equation.

$$\hat{H}\Psi = E\Psi \quad (1)$$

In this context, $\hat{H}$ represents the Hamiltonian operator, which is responsible for the total energy within the system. Ψ symbolizes the wave function, while E signifies the Eigen value resulting from the application of the Hamiltonian to the wave function, and DFT calculations utilize this equation [58]. The Hamiltonian, as depicted in equation (2), encompasses both the electron and nucleus energy within an atom.

$$\hat{H} = \hat{H}_e + \hat{H}_n \quad (2)$$

According to the Born-Oppenheimer approximation [59], the slower movement of the nucleus, due to its higher mass compared to electrons, allows for the separation of atomic nucleus dynamics:

$$(\hat{H}_e + \hat{H}_n)\Psi_n\Psi_e = E\Psi_n\Psi_e \quad (3)$$

$$\hat{H} = -\nabla^2 + V_{NN} + U_{ee} + V_{Ne} + V_{xc} \quad (4)$$

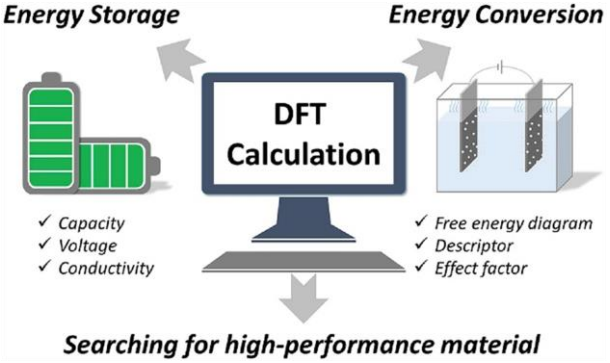

Figure 1. DFT simulation applications. Reprinted from Ref [60]. Licensed under CC BY-NC-ND 4.0 DEED [1].

[1] https://creativecommons.org/licenses/by-nc-nd/4.0/

The energy operator $\hat{H}_e$ of the electronic component is divided into three parts: the electrons' kinetic energy (T), the potential energy involving all the nuclei (V_{NN}), and three types of potential energy contributions—internal potential energy resulting from electron-electron repulsion (U_{ee}), external potential energy arising from electron-nuclei attraction (V_{Ne}), and the exchange and correlation potential energy (V_{xc}). The latter accounts for the impact of the Pauli exclusion principle and spin effects. The Schrödinger equation for a system with several electrons is based on the (5) equation. The positions of electrons are represented by r_1, r_2, r_3, $r_4 \ldots r_N$, corresponding to electrons numbered 1, 2, 3, 4…N, respectively. When solving the Schrödinger equation for each electron, the total electronic energy is computed using 3N variables (x, y, z). In the context of calculating molecules, the objective is to discover a wave function that reduces the system's energy. This reduction is achieved by minimizing the expectation or average value of the Hamiltonian. Consequently, wave functions are chosen randomly in a trial-and-error manner for calculations until the energy reaches its minimum point.

$$\hat{H}\Psi_e(r_1, r_2, r_3, r_4 \ldots r_N) = E\Psi_e(r_1, r_2, r_3, r_4 \ldots r_N) \quad (5)$$

$$E = \min_{\psi} < \psi|\hat{H}|\psi > \quad (6)$$

The solution of the many-body wave function in the Schrödinger equation is a complex and time-consuming process. To tackle this challenge, DFT was introduced by Hohenberg and Kohn in 1964 [61] and later refined by Kohn and Sham [62]. When applied to a system, DFT simplifies and makes its solution more realistic. Their proposition suggested that all electron-related information is encapsulated within the electron density, a function of three coordinates (x, y, and z). Instead of employing trial wave functions for energy minimization, they proposed minimizing the potential energy arising from interactions between nuclei and electrons by considering the electron density. This conceptual shift streamlined the approach to solving complex systems.

$$E = \min_n \{\int V_N(\vec{r})n(\vec{r})d^3\vec{r} + (-\nabla^2 + V_{NN} + U_{ee} + V_{xc})\} \quad (7)$$

2.1.2 Molecular Dynamics (MD)

MD is a computational technique used to model atomic and molecular movements and connections within a system. It is employed to analyze the structural [63], dynamic [64], and thermodynamic [65] characteristics of battery materials and interfaces, including diffusion [66], phase transitions [67], and mechanical actions [68] in electrodes and electrolytes. Additionally, MD is utilized to explore how temperature, pressure, electric fields, and other external factors impact battery stability and performance [69]. MD operates under the premise that atoms and molecules within a system adhere to classical laws of motion, such as Newton's second law, and interact through either empirical. This method solves the equations of motion for each atom or molecule in the system, producing trajectories and velocities of these particles over time. MD serves as a tool to investigate various properties of materials, encompassing structural, dynamical, and thermodynamic aspects, such as diffusion, phase transitions, reactions, and transport phenomena. In this context, a general method is outlined to derive the positions and velocities of a particle experiencing an effective potential over a duration. According to Newton's equations of motion, the force (F) acting on and the position (r) of atoms are governed by the interatomic potential (U_{eff}). The force is computed as the derivative of the potential with respect to the displacement (r), as depicted in Equation (8).

$$F = -\frac{dU_{eff}}{dr} \quad (8)$$

$$F = ma \quad (9)$$

$$r = \frac{1}{2}a\Delta t^2 + V_0\Delta t + r_0 \quad (10)$$

$$V = V_0 + a\Delta t \quad (11)$$

In continuation, employing the constant mass (m) of the atom, the acceleration (a) of the atom is determined using Equation 9, adhering to Newton's second law. Consequently, within a brief time interval (Δt), the minute alteration in acceleration can be disregarded. This allows for the derivation of each atom's position

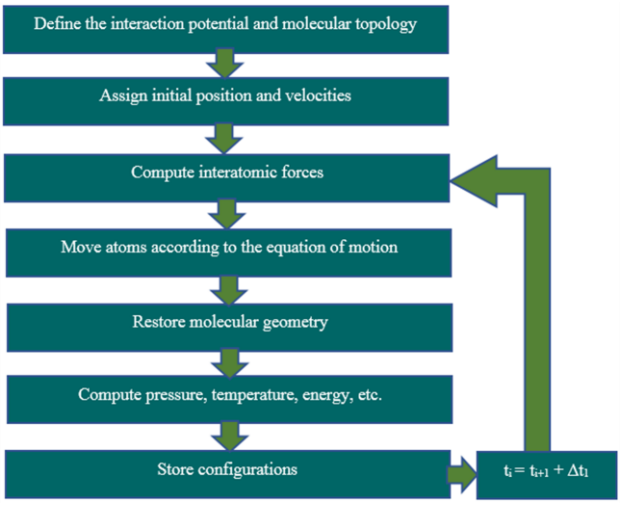

Figure 2. Flowchart of the molecular dynamics simulation procedure [70].

and velocity from the initial velocity (V_0), initial position (r_0), and the acceleration. The flowchart of the general steps of a molecular dynamic simulation is given in Figure 2.

Various numerical methods are utilized in MD simulations to compute particle trajectories. Additionally, it's crucial to appropriately set the system's size, enabling atoms to move as desired without extra constraints. Initial simulation settings encompass parameters like simulation dimensions, boundary conditions, and units, all of which are integral details to consider.

The numerical analysis involves employing the equation of motion with a short time increment, often referred to as the time step (Δt), to predict the position of atoms. The Taylor Series expansion for position as a function of time is expressed as:

$$\mathbf{r}(t+\Delta t) = \mathbf{r}(t) + \frac{dr(t)}{dt}\Delta t + \frac{1}{2}\frac{d^2r(t)}{dt^2}\Delta t^2 + \frac{1}{3!}\frac{d^3r(t)}{dt^3}\Delta t^3 + \cdots \quad (12)$$

Rewriting Equation (XI) from t to $t - \Delta t$ results in:

$$\mathbf{r}(t-\Delta t) = \mathbf{r}(t) - \frac{d\mathbf{r}(t)}{dt}\Delta t + \frac{1}{2}\frac{d^2r(t)}{dt^2}\Delta t^2 - \frac{1}{3!}\frac{d^3r(t)}{dt^3}\Delta t^3 + \cdots \quad (13)$$

Combining Equations (XII) and (XIII) to eliminate terms allows us to derive Verlet's algorithm for position, retaining terms larger than Δt^4:

$$\mathbf{r}(t+\Delta t) = 2\mathbf{r}(t) - \mathbf{r}(t-\Delta t) + \frac{d^2r(t)}{dt^2}\Delta t^2 + \cdots \quad (14)$$

To predict the position at $t + \Delta t$, the Verlet algorithm employs the positions at time t and $t - \Delta t$, alongside the acceleration derived from the interatomic potential U_{eff}. By subtracting Equation (XII) from Equation (XIII) and retaining terms larger than Δt^3, we derive:

$$\mathbf{r}(t+\Delta t) - \mathbf{r}(t-\Delta t) = 2\frac{dr(t)}{dt}\Delta t + \cdots \quad (15)$$

Therefore, the velocity at t can be obtained:

$$v(t) = \frac{\mathbf{r}(t+\Delta t) - \mathbf{r}(t-\Delta t)}{2\Delta t} \quad (16)$$

The method described allows for iterative updates of positions and velocities for each particle in the system over time, utilizing previous values to derive new positions and velocities until a complete trajectory is obtained. LAMMPS employs an algorithm similar to the Verlet Algorithm, enabling MD simulations to track atom movements.

Considering MD simulations necessitates integrating principles from statistical mechanics, incorporating parameters such as temperature (T), pressure (P), and volume (V). This incorporation ensures that our simulations mirror experimental conditions, enabling control over temperature, pressure, and volume.

Moreover, LAMMPS utilizes Martyna's paper [71] to incorporate additional ensemble effects into particle motion, beyond the traditional Hamiltonian treatment. While the paper's details are intricate, the fundamental concepts can be summarized as follows:

The approach begins with the classical Hamiltonian equation:

$$\mathbf{H}_{\text{Classical}}(\{\mathbf{r}_i\},\{\mathrm{P_i}\}) = \sum_i \frac{\mathrm{P_i}^2}{2\mathrm{m_i}} + \mathrm{U_{eff}}(\{\mathbf{r}_i\}) \tag{17}$$

The Hamiltonian characterizes a system comprised of multiple particles. The total energy within the system encompasses the summation of kinetic energies across all particles and the collective effective potential energy of the entire system. Kinetic energy is contingent on the momentum ($\mathrm{P_i}$) of each atom indexed as i, while potential energy relies on the positions of all particles (r_i). Here, mi represents the mass of an atom.

In MD simulations, the total effective Hamiltonian of the system includes an additional statistical term, which likely accounts for factors such as ensemble effects or statistical contributions to the dynamics of the particles.

$$H_{\text{eff}} = H_{\text{classical}} + H_{\text{ensemble}} \tag{18}$$

$$H_{eff} = \sum_i \frac{{P_i}^2}{2m_i} + U_{eff}(\{r_i\}) + \frac{{p_\epsilon}^2}{2W} + \frac{{p_\xi}^2}{2Q} + \left(N_f + 1\right)kT\xi + P_{ext}V \tag{19}$$

In this context, the variables are defined as follows: V represents the volume of the simulation box, P_{ext} stands for the targeted equilibration pressure, and P_{int} is a function influenced by momentum and forces, varying over time. p_ϵ denotes the barostat momentum, while p_ξ represents the thermostat momentum with a thermostat position ξ. Both barostatic and thermostatic variables possess parameters (W and Q, respectively) to regulate equilibration time. Notably, N signifies the number of particles, d signifies dimensionality, and N_f denotes degrees of freedom. The equations of motion formulated by Hoover in this scenario are outlined as follows:

$$\frac{\mathrm{d}r_i}{\mathrm{dt}} = \frac{P_i}{m_i} + \frac{p_\epsilon}{W} r_i \tag{20}$$

$$\frac{\mathrm{d}P_i}{\mathrm{dt}} = F_i - \frac{p_\epsilon}{W} P_i - \frac{p_\xi}{Q} P_i \tag{21}$$

$$\frac{\mathrm{dV}}{\mathrm{dt}} = \frac{dV p_\epsilon}{W} \tag{22}$$

$$\frac{\mathrm{d}p_\epsilon}{\mathrm{dt}} = \mathrm{dV}(P_{int} - P_{ext}) - \frac{p_\xi p_\epsilon}{Q} \tag{23}$$

$$\frac{\mathrm{d}\xi}{\mathrm{dx}} = \frac{p_\xi}{Q} \tag{24}$$

$$\frac{\mathrm{d}p_\xi}{\mathrm{dt}} = \sum_{i=q}^{N} \frac{P_i^2}{m_i} + \frac{p_\epsilon^2}{2W} - \left(N_f + 1\right)kT \tag{25}$$

Martyna elucidates that according to Hoover's equations of motion, the average of the time derivative for both the barostat and thermostat momenta tends towards zero when the system reaches equilibrium. This occurs when the internal pressure averages to the external target pressure, and the temperature aligns with the typical relation to the average kinetic energy. Consequently, LAMMPS leverages these equations of motion to govern the NPT ensemble, a scenario where the number of particles (N), the pressure (P), and the temperature (T) are controlled. This control is achieved through a numerical evaluation facilitated by a modified version of the Verlet integration method. This modified approach ensures the system maintains the desired pressure and temperature conditions while undergoing simulations.

2.1.3 Molecular Docking (MDK)

Molecular Docking (MDK) is a computational approach utilized to anticipate the preferred alignment and binding strength among multiple molecules. It aids

in refining the molecular architectures of organic electrodes and electrolytes for batteries [72], focusing on aspects like redox potentials, solvation impacts, and rates of charge transfer [73, 74]. The principles and assumptions underlying MDK in LIBs revolve around predicting the binding affinity and orientation of lithium ions within the molecular structures of electrodes or electrolytes.

$$\begin{aligned} &MDK \\ &= Force\ Fields \\ &+ Molecular\ Recognition \\ &+ Conformational\ Flexibility \\ &+ Docking\ Algorithms \\ &+ Scoring\ Functions + Assumptions \\ &+ Validation \end{aligned} \tag{26}$$

This equation dissects MDK into its core components.

Force Fields: Models atomic interactions within molecules, calculating their energies.

Molecular Recognition: Presumes specific binding sites for lithium ions in molecular structures, predicting these sites and understanding their interactions.

Conformational Flexibility: Incorporates the ability of molecular structures to adjust for lithium ions, affecting binding.

Docking Algorithms: Employed to explore various lithium ion placements within molecules for optimal binding.

Scoring Functions: Evaluate and score lithium ion positions based on electrostatics, steric hindrance, and hydrogen bonding.

Assumptions: Encompasses suppositions about electrolyte behavior and stability, impacting prediction accuracy.

Validation: Compares MDK forecasts against real-world data for accuracy.

This formula succinctly outlines the foundational aspects of Molecular Docking in LIBs.

2.1.4 Molecular Self-Assembly (MSA)

MSA is the natural arrangement of molecules into structured forms via non-covalent forces like hydrogen bonds and van der Waals interactions. This process is instrumental in crafting nanostructured elements for batteries, like electrode nanowires, nanotubes, and nanosheets [75]. MSA plays a pivotal role in dictating the shape, texture, and function of battery materials, elevating their performance, stability, and safety [76]. The fundamental principles guiding MSA within LIBs can be summarized in this way:

Non-Covalent Interactions: These interactions, such as hydrogen bonding, van der Waals forces, and π-π stacking, direct the natural assembly of molecules.

Energetic Favorability: This principle highlights that assembled structures aim for lower-energy states, minimizing overall free energy.

Molecular Design: Emphasizes the significance of crafting molecules with matching shapes and chemical traits for easier self-assembly into desired structures.

Kinetic Control: Acknowledges that the speed of assembly, influenced by molecular movement rates or templating effects, affects the final structure.

Thermodynamics and Equilibrium: Encompasses the principles of thermodynamics and equilibrium, ensuring the assembly process reaches a stable state with minimized free energy.

Equations characterizing MSA in LIBs often involve formulations concerning intermolecular forces, potential energy landscapes, and free energy calculations derived from statistical mechanics and thermodynamics. These equations encapsulate the core concepts directing the process of molecular self-assembly in battery applications.

2.2 Continuum models

2.2.1 Doyle-Fuller-Newman (DFN)

DFN model is a physics-rooted framework delineating transport and reaction processes within a LIB cell. Employing partial differential equations (PDEs), it embodies mass, charge, and energy conservation in electrodes and electrolytes. This model adeptly

captures spatial and temporal shifts in variables like temperature [77], concentration, potential [78], and current density [78], offering valuable perspectives on battery functionality, wear, and safety. Yet, the DFN model encounters challenges in defining and validating numerous model parameters, posing hurdles in their applicability, estimation, and verification. The Pseudo-Two-Dimensional (P2D) Model simplifies the DFN model by presuming uniform transport and reactions across the current collectors' perpendicular direction, reducing computational intricacies. While the P2D model adeptly tracks variations in electrode and electrolyte thickness and length [79], offering credible battery forecasts, it might overlook vital occurrences perpendicular to this direction, like thermal gradients, concentration polarization, and interfacial impedance [80]. The Single-Particle Model (SPM) is a streamlined adaptation of the DFN model, envisioning electrodes as uniform spherical particles with consistent properties. Employing ordinary differential equations (ODEs) instead of partial differential equations (PDEs), the SPM model curtails computational expenses while swiftly approximating battery voltage and state of charge [81]. The Single-Particle with Electrolyte (SPE) Model, an adaptation of the Single-Particle Model (SPM), integrates electrolyte transport and potential. By accommodating concentration polarization and interfacial impedance, disregarded in the SPM, the SPE model offers an improved assessment of battery voltage and state of charge [82]. DFN operates on specific principles and assumptions: The battery comprises three porous electrodes (anode, cathode, and separator) interconnected by an electrolyte solution. The battery functions under consistent and uniform temperature conditions (isothermal). It operates under constant and known current conditions (galvanostatic). Additionally, the battery adheres to dilute solution theory, where the electrolyte concentration is sufficiently low to ignore activity coefficients and solution volume changes.

Moreover, the battery adheres to ideal solid solution theory, maintaining uniform solid phase concentration irrespective of lithium insertion or extraction. It follows Butler-Volmer kinetics, where the interfacial reaction rate correlates with the difference between electrode potential and equilibrium potential. Lastly, the battery assumes spherical particle behavior, with active material particles in the electrodes considered spherical and homogeneous.

The governing equations of DFN can be written as follows:

Charge conservation:

$$\frac{\partial i_{\mathrm{e,k}}}{\partial x} = \begin{cases} j_{\mathrm{k}}, & \mathrm{k} = \mathrm{n,p}, \\ 0, & \mathrm{k} = \mathrm{s}, \end{cases} \tag{27}$$

$$\begin{aligned} & i_{\mathrm{e,k}} \\ & = \epsilon_{\mathrm{k}}^{\mathrm{b}} \hat{\kappa}_{\mathrm{e}} \kappa_{\mathrm{e}}\left(c_{\mathrm{e,k}}\right)\left(-\frac{\partial \phi_{\mathrm{e,k}}}{\partial x}\right. \\ & \left. + 2(1-t^{+})\frac{\partial}{\partial x}\left(\log\left(c_{\mathrm{e,k}}\right)\right)\right), \\ & \mathrm{k} \in \{\mathrm{n,s,p}\}, \end{aligned} \tag{28}$$

$$\begin{aligned} & I - i_{\mathrm{e,k}} \\ & = -\sigma_{\mathrm{k}}\frac{\partial \phi_{\mathrm{s,k}}}{\partial x}, \end{aligned} \tag{29}$$

Molar conservation:

$$\begin{aligned} \mathcal{C}_{\mathrm{e}}\epsilon_{\mathrm{k}}\gamma_{\mathrm{e}}\frac{\partial c_{\mathrm{e,k}}}{\partial t} &= -\gamma_{\mathrm{e}}\frac{\partial N_{\mathrm{e,k}}}{\partial x} \\ &\quad + \mathcal{C}_{\mathrm{e}}\frac{\partial i_{\mathrm{e,k}}}{\partial x}, \\ \mathrm{k} &\in \{\mathrm{n,p}\} \end{aligned} \tag{30}$$

$$\begin{aligned} N_{\mathrm{e,k}} &= -\epsilon_{\mathrm{k}}^{\mathrm{b}} D_{\mathrm{e}}\left(c_{\mathrm{e,k}}\right)\frac{\partial c_{\mathrm{e,k}}}{\partial x} \\ &\quad + \frac{\mathcal{C}_{\mathrm{e}} t^{+}}{\gamma_{\mathrm{e}}} i_{\mathrm{e,k}}, \\ \mathrm{k} &\in \{\mathrm{n,p}\} \end{aligned} \tag{31}$$

$$\begin{aligned} & \mathcal{C}_{\mathrm{k}}\frac{\partial c_{\mathrm{s,k}}}{\partial t} \\ & = \frac{1}{r_{\mathrm{k}}^{2}}\frac{\partial}{\partial r_{\mathrm{k}}}\left(r_{\mathrm{k}}^{2}\frac{\partial c_{\mathrm{s,k}}}{\partial r_{\mathrm{k}}}\right), \\ & \mathrm{k} \in \{\mathrm{n,p}\}. \end{aligned} \tag{32}$$

Electrochemical reactions:

$$j_{\mathrm{k}} = j_{0,\mathrm{k}}\sinh\left(\frac{\eta_{\mathrm{k}}}{2}\right), \tag{33}$$

$$j_{0,\mathrm{k}} = \frac{\gamma_{\mathrm{k}}}{\mathcal{C}_{\mathrm{r,k}}}c_{\mathrm{s,k}}^{1/2}(1-c_{\mathrm{k}})^{1/2}c_{\mathrm{e,k}}^{1/2}\Big|_{r_{\mathrm{k}}=1}, \tag{34}$$

$$\eta_{\mathrm{k}}\& = \phi_{\mathrm{s,k}} - \phi_{\mathrm{e,k}} - U_{\mathrm{k}}\left(c_{\mathrm{s,k}}\big|_{r_{\mathrm{k}}=1}\right), \tag{35}$$

2.2.2 Thermal model

A thermal model is a mathematical tool that describes how heat moves and temperatures spread within a battery setup. It plays a key role in predicting how temperature affects battery performance, wear and tear, and safety, also helping to develop and enhance systems that manage battery temperature using cooling or heating techniques. Battery thermal models come in different types: lumped parameter [83], distributed parameter [84], and coupled electro-thermal models [85]. Lumped parameter models assume uniform battery temperatures and use ordinary differential equations (ODEs) to illustrate heat balance. Distributed parameter models consider temperature changes across space, utilizing partial differential equations (PDEs) or finite element methods (FEMs) to detail heat movement through conduction and convection. Coupled electro-thermal models combine thermal with electrical or electrochemical models, capturing how heat generation interacts with battery behavior. In thermal simulations, addressing temperature involves solving the energy equation, which holds significant importance within the simulation framework.

The energy equation is fundamental:

$$\underbrace{\rho c_\mu \frac{\partial T}{\partial t}}_{I} + \underbrace{\rho c_\mu U_i \frac{\partial T}{\partial x_i}}_{II} = \underbrace{-P \frac{\partial U_t}{\partial x_i}}_{II} + \underbrace{\lambda \frac{\partial^2 T}{\partial x_i^2}}_{IV} \underbrace{-\tau_{ij} \frac{\partial U_j}{\partial x_i}}_{V} \quad (36)$$

Where:

I: Energy changes with time

II: Convection term

III: Pressure work

IV: Diffusion term

V: Dissipation term

When incorporating fluid motion within the simulation, governing equations include the continuity equation (XXI) and the Navier-Stokes (XXII) equation:

$$\frac{\partial \rho}{\partial t} + \nabla \cdot \left(\rho \vec{V}\right) = 0 \quad (37)$$

$$\frac{\partial \mathrm{u}}{\partial t} + (\mathrm{u} \cdot \nabla)\mathrm{u} = -\nabla w + \nu \nabla^2 \mathrm{u} + \mathrm{g} \quad (38)$$

It's important to emphasize that boundary conditions vary based on the specific simulation scenario. However, fundamentally, these conditions revolve around determining the heat transfer at the boundary.

3. Computational methods and modeling techniques for simulating COF based lithium-ion batteries

3.1 key performance parameters to evaluate COF-based lithium batteries

A range of electrochemical characterization methods have been devised to examine the characteristics of new COF-based cathode, anode, and electrolyte materials and to track how material alterations affect battery performance [86]. The next section contains a summary of the most widely used methods for electrochemical characterization [34].

3.1.1 Cyclic voltammetry

The electrochemical and chemical reversibility of redox active COF electrode materials can be studied using cyclic voltammetry (CV), a widely used technique since it is simple to use and yields useful data. The working electrode of a CV experiment receives a potential that is applied and linearly scanned to the switching potential, which is a predefined value. The scan is reversed, and the applied potential is set back to its starting value at the switching potential. A core-shell structured magnetic COF (Fe_3O_4@TAPB-DMTP-COFs) was created by Yang Wang [87] and colleagues using an easy-to-follow assembly procedure. The Fe_3O_4@TAPB-DMTP-COFs/GCE showed the largest peak current of luteolin on the TAPB-DMTP-COFs/GCE. Results from the CV experiment is presented as applied voltage vs. current response. During the scan, the current response is obtained [88].

The scan rate (V/s) is a crucial characteristic that needs to be disclosed for every CV experiment. The speed at

which the potential is linearly scanned between the initial and switching potentials is indicated by the scan rate [89]. According to solid-state CV measurements, Anqi Wang [90]. prepared conventional coin cells with lithium foil anodes and cathodes made from slurries of each polymer with carbon black and PVDF binder in anhydrous NMP. PIM-TMTripMQ exhibited four pairs of well-resolved redox peaks with E1/2 values of 2.11, 2.37, 2.64, and 2.84 V vs Li/Li^+, respectively. For electrochemically reversible processes, the peak current should grow linearly with the square root of scan rate, as per the Randles-Sevick equation [23]. Electrochemical species diffusion coefficients can be computed by detecting peak current and adjusting the scan rate. The peak currents, the voltages at which they occur, and the peak spacing are significant values on a CV plot. On the CV plot, the current peaks show the movement of electrons, and the voltage at which the peak appears is related to a particular redox process. Yi Meng [91] utilized varying scan rates to analyze the CV of Py-COF/S in order to investigate the cause behind its superior electrochemical performance compared to BP2000/S. It was shown that the lithiation of sulfur and the delithiation of lithium sulfides corresponded to two cathodic peaks and one anodic peak. Formal reduction potentials of a system can be quickly and precisely estimated using the peak locations on a CV plot.

The system's electron transfer kinetics are referred to as electrochemical reversibility. Electrochemically reversible systems have low barriers to electron transport, while electrochemically irreversible systems have high barriers and slow electron transfer reactions. The separation of the cathodic and anodic peak potentials on the CV plot indicates the electrochemical reversibility [92]. A one-electron transfer process has a peak separation of 59 mV in an electrochemically reversible solution. A higher barrier to electron transfer indicates a greater peak separation, indicating the need for a higher negative (positive) potential to facilitate reduction (oxidation) processes. The ability of a chemical species to reoxidize after reduction and remain stable is known as chemical reversibility. For instance, the two unique anodic and cathodic peaks on the CV curves of Co-MOF/120 and Co-MOF/150, obtained at 0.005, 0.01, 0.02, 0.05, and 0.1 $V.s^{-1}$, correspond to their two subsequent lithiation/delithiation phases, demonstrating the reversible electrochemical process [23]. Co-MOF/150 has a smaller anodic and cathodic peak separation than Co-MOF/120, indicating a reduced charge transfer barrier in Co-MOF/150. The CV plot displays a single reduction (oxidation) peak with no oxidation (reduction) peak on the return scan, indicating that a COF material is chemically irreversibly oxidized or degrades after reduction (oxidation) and cannot be oxidized (reduced). The success of rechargeable LIBs is largely dependent on the electrochemical reversibility of the lithiation/delithiation processes.

3.1.2 Electrochemical impedance spectroscopy

Electrochemical impedance spectroscopy (EIS) is a commonly used technique to measure cell impedance and ascribe impedances to various features of an electrochemical cell. With an EIS, a small AC potential (5-15 mV) of a given frequency is applied to a working electrode, and the AC current response is measured. The frequency of the AC potential is scanned in the mHz-to-MHz range [93]. To create redox-active polymers of intrinsic micro porosity (PIMs) with rapid lithium-ion transport and storage, Anqi Wang [90]. described a novel molecular engineering technique. PIMs have an open network of sub-nanometer pores and readily accessible carbonyl-based redox sites. The highly interconnected pores of redox-active PIMs increased Li^+ ion diffusion, as demonstrated by tests using EIS and CV. Real (resistive) and imaginary (reactive) components of the impedance can be distinguished using the AC phase shift that exists between the applied potential and the current response. A Bode (frequency vs. impedance) or Nyquist (real impedance vs. the negative of imaginary impedance) graphic is frequently used to depict EIS data. Nyquist plots, which are easier to read visually, are more frequently used in literature than Bode plots, which offer valuable information on frequency. A typical Nyquist plot shows a line with a 45° slope in the low frequency zone that represents the diffusion of a species toward or away from an electrode surface, known as Warburg impedance, and semicircles in the high frequency region that correspond to charge transfer processes [94]. Total impedance can be divided into discrete components that correspond to different properties in an electrochemical cell by fitting EIS data with an equivalent circuit. A multi-

component equivalent circuit model can be used to perfectly fit EIS data; nevertheless, it is more crucial that each circuit element matches a significant feature in the cell [95].

For instance, LiCON-TFSI, a spiroborate-linked COF (ICOF) that functions as a solid-state electrolyte, exhibits a semi-circle at high frequency and a sharp spike at low frequency in its Nyquist plots [7]. which demonstrate the capacitive nature of the interface between the electrode and electrolyte. Usually, a single cell has several processes operating in the same frequency range. This can cause the high frequency range semicircles to become depressed, and in analogous circuit models, constant phase elements are sometimes used in place of capacitors to simulate this. Solid-state electrolyte (SSE) research requires the use of EIS. PoojaVadhva [96] reviewed the pertinent EIS theory for ASBs, then discussed electrode/cell arrangements for electrochemical measurements and approaches to modeling the impedance spectrum. He found out There are currently insufficiently thorough EIS investigations on all-solid-state Li-S and Li-air batteries, and more device-level research is needed to clarify any broad-spectrum assignment methodologies.

3.1.3. Cycling

Cycling, which is the act of charging and discharging an electrochemical cell, is usually the initial experiment carried out to assess novel electrode materials. The development of high-capacity electrode materials is essential to produce energy-dense batteries, and cycling quantifies the variations in capacity performance caused by the recurrent intercalation and deintercalation of lithium in electrode materials. An electrode material's theoretical capacity, which is determined by the material's molecular weight and the quantity of lithium it can hold, is compared to the observed capacity of the material during cycling. Many researchers examined capacity of lithium ion batteries using cycling [97]. Qing Ai [98] used silicon nanoparticles as artificial solid electrolyte interphase (SEI) for the Si electrode by coating them with lithium-conducting COF. After examining the cycling performances of Si@COF electrodes with various mass ratios, it was discovered that the Si electrodes' cycling stability had significantly increased. By using in situ growth on micro-sized siloxene, Yuchan Zhang [99] created a thin, porous coating layer for COFs. With 96% capacity retention at 8 A g^{-1} over 1500 cycles, the designed siloxene exhibits exceptional electrochemical performance thanks to the inherent ionic conductive and electrolyte compatible advantages of COF.

3.1.3.1. Galvanostatic cycling

Cycling is usually done galvanostatically, or with a continuous current, in research settings. Cell performance is greatly impacted by the applied current, and galvanostatic cycling permits total control over applied current, whereas potentiostatic (constant voltage) cycling does not. Galvanostatic cycling involves applying a steady current to the cell's working electrode for a set period of time, or until a specific potential limit is reached. Once a second potential or time limit is reached, the applied current's polarity is switched. In order to maximize the practical capacity of the materials utilized in the cell, the voltage stability window of such materials determines the potential limitations for galvanostatic cycling [97]. A galvanostatic cycling experiment's constant current is determined by C-rates, which normalize the current to the working electrode's capacity. A 1C rate means that the applied current could fully charge or discharge the electrode in an hour; higher C-rates mean a faster charge; 2C means a ½ hour charge or discharge; and lower C-rates mean a slower charge (C/2 = 2 h). High-rate cycling performance establishes how quickly a battery can charge, so it is important to maintain performance at high C-rate. Generally, the cell capacity decreases at higher rates due to kinetic limitations [100]. In rate tests, a kind of galvanostatic cycling experiment, the cell is cycled at a low C-rate (C/20) for a few cycles, and then the current is progressively increased to a high rate (5-10 C). The current returns to a low rate following high rate cycling. In Yucheng Wen group work, a custom-designed COF from 1,3,5-tris(4-aminophenyl) benzene and 2,5-dimethoxybenzene-1,4-dialdehyde was coated on a commercial polymer separator (PS) to create a unique polymer separator that can control the movement of lithium ions and TMIs. At 0.1C, the modest discharge rate yielded a high specific capacity of 310 mAh.g^{-1}. At 1C, the specific capacity was still greater than 190 mAh.g^{-1}. The capacity increased to

300 mAh.g^{-1} as the temperature dropped to 0.1C, indicating that the separator material is stable [34].

3.1.3.2. Cycle Life and Coulombic Efficiency

Usually, galvanostatic cycling continues until the cell reaches the end of its cycle life. Research groups define end of cycle life differently, but generally speaking, it refers to a discharge capacity that is 80% or less of the initial discharge capacity [101]. Cycle number is plotted against charge and discharge capacity in cycle life plots, which also usually include a second y-axis that shows the Coulombic efficiency (CE) for each cycle. CE, which is calculated by dividing the discharge capacity by the charge capacity that came before it, indicates how well charges are transferred within the cell [102]. Extensive lifetimes for LIBs that need to operate for thousands of cycles are made possible by high CE (˜99.9%) [103]. After 100 cycles, even a cell with a constant CE of 99% would only retain 37% of its initial capacity (99%100 = 37%). Note that extended cycle life experiments (10,000 cycles at 5C=167 days) can take several months to finish [104]. End of cycle life will usually happen more quickly for innovative systems under study (between 100 and 1000 cycles) but employing lower C-rates also lengthens the testing period. At a high current density of 2000 mA g^{-1}, the Si@COF exhibits a capacity of 1864 mAh.g^{-1}, and after 1000 cycles, an outstanding capacity retention of more than 60% is reached. In addition, a remarkable average CE of 99.6% is attained, demonstrating the stability of COF coating as an artificial surface equivalent of SEI [97].

3.1.3.3. Charge/discharge curves

With the known applied current and observed voltage values, charge/discharge curves, also known as voltage profiles, can be shown for each cycle. The capacity for the cycle is shown by the length of the curve, which is typically represented as specific capacity, duration, or stoichiometry vs. voltage (longer equals higher capacity). An electrochemical cell's voltage profile is influenced by its cycle number, temperature, and rate. The voltage profile's shape sheds light on the charge/discharge process in addition to capacity data. One or more voltage plateaus can be seen in voltage profiles; these can be sloping (signaling the development of a solid solution) or flat (signaling a two-phase reaction). Research to comprehend the emergence of different phases during the charge/discharge process is aided by the study of voltage profiles [105]. The kinetic limit, shown by steep polarization represented by vertical lines, is the point at which the electrode reaction can no longer consume the applied current. Three distinct discharge plateaus, located around 3.20-2.47 V, 2.47-2.11 V, and 1.4-1.2 V, and can be identified from the fully reversible galvanostatic charge/discharge curves. Due to the creation of the SEI film, the first cycle CV curve displays an additional anodic peak at 3.36 V in comparison to the subsequent cycles. The redox process is shown to be reversible in the second and third CV curves. With a high coulombic efficiency of 98.4% and a high starting capacity of 494 mA h g^{-1}. These findings show that BQ_1-COF is a very reversible cathode material for LIBs. The cathode shows an extremely high capacity of 502.4 mA h g^{-1}, which is noteworthy [106].

3.2 Modeling and simulation of COF based anodes

To simulate COFs, various computational methods have been proposed. One approach involves utilizing Density Functional Tight Binding (DFTB) and neural network potentials to achieve DFT accuracy at a lower computational cost [107]. This strategy has shown promise in characterizing host-guest interactions in metal- and COFs. Additionally, MD simulations and DFT calculations have been used to elucidate the formation of a 2D soft COF membrane, demonstrating the potential of simulations in understanding the dynamic behavior of COFs [108]. Furthermore, the design of three-dimensional COF membranes for organic solvent nanofiltration has been explored, highlighting the potential of COFs in revolutionizing membrane materials and technologies [109].

Moreover, DFT computations have rationalized the enhanced surface area and reduced pore collapse of methylated, imine-linked COFs, demonstrating the utility of DFT in understanding the structural properties of COFs [110]. Additionally, the development of metal–covalent organic frameworks (MCOFs) has been proposed to address the shortcomings of traditional COFs by incorporating active metal species atop highly stable COF backbones

[111]. Furthermore, the application of dynamic covalent chemistry concepts towards tailored COF nanomaterials has been reviewed, emphasizing the importance of computational design and simulation in the development of COFs [112].

The use of Vienna ab initio Simulation Package (VASP) software for simulating COFs as anode materials for batteries has gained significant attention in recent years. VASP is a widely used software for performing electronic structure calculations and quantum mechanical molecular dynamics simulations, particularly in the field of materials simulation and computational material science research [113]. The application of VASP in simulating the electronic structure and properties of COFs as anode materials can provide valuable insights into their performance and behavior in battery systems. Lei Fang [114] Performed The spin-unrestricted DFT calculations by the VASP and the generalized gradient approximation with the Perdew-Burke-Ernzerhof (GGA-PBE) exchange-correlation functional employed to treat the electron–electron interactions. The calculations show that the structural framework of NUS-2 can maintain stable and unchanged till the number of intercalated Li atoms increases up to 14 for its monolayer super cell, and the corresponding electric conductivity is getting better and better as the intercalation of more Li atoms.

HyperChem is a sophisticated molecular modeling environment that is known for its quality, flexibility, and ease of use [115]. The use of HyperChem in computational analysis of atomic binding energy for composite membranes, molecular generation models, molecular reconstruction, and corrosion studies, among others, demonstrates its versatility and wide applicability in the field of chemistry and materials science. Additionally, the references also discuss the use of HyperChem in molecular modeling, quantum chemistry simulations, and quantum computational chemistry, highlighting its significance in cutting-edge research areas.

The study by Yusuf [116] is directly relevant as it focuses on a theoretical study using the PM3 semi-empirical computational method, which aligns with the task of determining the band gap of a complex compound using HyperChem. The study provides a specific example of the software's application in theoretical chemistry. The study by Rosli et al [117] is relevant as it demonstrates the use of HyperChem in computational analysis of atomic binding energy for composite membranes, showcasing the software's application in material science and computational chemistry.

The study by Paredes-Doig *et al.* [116] is pertinent as it discusses the interaction of metallic ions onto activated carbon surfaces using computational chemistry software, specifically mentioning the use of HyperChem to corroborate surface information. This highlights the software's role in studying surface properties and interactions. The study by Sabet & Jafroudi [118] is applicable as it involves the use of HyperChem for calculating physicochemical parameters, which is relevant to the computational study of chemical compounds and aligns with the task of theoretical analysis using HyperChem. The study by Streif [119] is not directly relevant as it primarily discusses solving quantum chemistry problems with a D-Wave quantum annealer, which is not directly related to the theoretical study using HyperChem for determining the band gap of a complex compound. In conclusion, the references provide comprehensive insights into the diverse applications of HyperChem in computational chemistry, molecular modeling, and quantum chemistry simulations. The selected references demonstrate the relevance and significance of HyperChem in addressing various research questions in the field of chemistry and materials science.

Jianjun Zhao [120] simulated results of synthetizing three kinds of phthalocyanine-based COFs, NA-NiPc (4-nitronickel phthalocyanine+4-aminonickel phthalocyanine), PPDA-NiPc (4-nitronickel phthalocyanine + p-phenylenediamine) and DAB-NiPc (4-nitronickel phthalocyanine+4,4′-diaminobiphenyl), with different pore sizes by a catalyst-free coupling reaction and simulated results after optimizing the geometric conformation by HyperChem software.

3.3 Modeling and simulation of COF-based cathodes

In the discharging phase, the anode releases lithium ions which then traverse the separator and ultimately become embedded in the cathode. This process generates an external current that powers electrical

devices. Conversely, in the charging phase, an external voltage is necessary to facilitate the thermodynamically-uphill reaction. Lithium ions move back and forth between the two active electrodes in a rocking-chair fashion. Enhancing the energy density is a crucial prerequisite for advanced LIBs, hence it is imperative to make necessary improvements and modifications in all three aspects [19]. The energy density, rate capability, and cycle life of LIBs are interconnected with the chemical properties of the cathode materials [121]. Specifically, the rate capability is influenced by the presence of a cathode electrode that exhibits high electronic and ionic conductivities, thereby impacting the overall performance of the battery. Experimental studies have demonstrated that heteroatom doping and surface coating can effectively modify cathodes [122-128]. Other suggested materials for cathode development include layered transition metal oxides, olivines, spinels, and organic compounds with flexible morphological structures [129-134]. Notably, COFs have shown promising potential as electrode materials. COFs represent a novel category of materials wherein distinct organic groups are covalently linked to form a periodic network. These exceptional attributes empower COFs to possess meticulously engineered chemical structures and enable the creation of uniformly distributed lithophilic sites. Extensive research on COFs as electrode materials in Li-S batteries in recent years has revealed their potential as high-performance cathode materials, making them strong contenders in the field [135-137].

JongTae Yoo *et al.* [138] in 2016 investigate a microporous COF net on mesoporous CNT net hybrid architecture as a new class of molecularly designed, hierarchical porous chemical trap for lithium polysulfides in Li-S batteries. Theoretical investigation using DFT calculation was conducted to analyze the impact of pore size and chemical affinity of microporous COF nets, which possess boroxine and boron ester groups, on the adsorption of Li_2S_x. The study particularly focused on the adsorption energies of insoluble Li_2S. The total adsorption energies include bond formation (E_{bond}), reconstruction of the host structures of CNT, COF-1 and COF-5 (E_{recon}) and structural change of Li_2S_x guests (E_{Li2Sx}) are reported [138], and computing as the following express:

$$E_{ads} = E_{bond} + E_{recon} + E_{Li2Sx} \quad (39)$$

The LDOS of Li_2S-adsorbed COF-1, it can be observed that the peaks of Li_2S and boron of COF-1 overlap with each other. This suggests the mixing of p- and s orbitals in the HOMO-1 and HOMO-2 levels, respectively [138].

Zhubing Xiaoa and colleagues [139] have studied the lithiophilic and sulfiphilic interactions of lithium PSs with the triazine and boroxine units in the TB-COF compound. The presence of both units restricts the movement of PSs within the cathodes and reduces the shuttle effect of PSs. The Materials Studio software package was employed to generate the crystal model. The binding energy between the sulfur species and TB-COF was calculated using DFT. The binding energies of solid-state lithiation products, in the range of -180.75 to 440.80 kJ mol^{-1}.The Mulliken charge variations observed throughout the lithiation process indicate a more pronounced chemical bonding between B and S compared to N and Li. The comparison of atomic partial density of states (PDOS) on boroxine and triazine rings before and after Li_2S adsorption suggests a p-p orbital interaction between S and B following the absorption of Li_2S on the boroxine ring. Additionally, there is an s-p orbital interaction between Li and O, which aligns with the XPS results [139].

In recent years, the potential of 2D COFs as electrode materials in batteries and supercapacitors has been investigated due to their varied functionality and structural adaptability [140-145]. The CNT is shielded by a layer of covalent organic nanosheets, which serves as a porous chemical trap, effectively hindering the dissolution of polysulfide from the cathode into the liquid electrolyte. Ruth Gomes and Aninda J. Bhattacharyya carried out DFT calculations were employed in the DMol3 package to investigate the nonbonded interaction between the polysulfides and COF surface. The adsorption energies (E_{ads}) of each polysulfide species to the COF framework is calculated according to the formula $E_{ads} = E_{total} - E_{COF} - E_{PS}$, where E_{total} is the total energy of the adsorbed system, and E_{COF} and E_{PS} are the energies of individual COF and polysulfide molecules. The absorption energies of the polysulfides (Li_2S_4, Li_2S_6, and Li_2S_8) on the COF surface are obtained to be −4.757, −4.579, and −4.269 eV, respectively. the PXRD data effectively

demonstrate that the COF maintains its 2D hexagonal structure while being synthesized over the CNTs with open ends [146]. Additionally, the PXRD pattern of CNT-CON/S exhibits peaks corresponding to CNT-CON, as well as distinctive peaks of elemental sulfur, suggesting the inclusion of sulfur in the material [147, 148].

Tianyu Qiu et al, synthesized a series of fluorinated COFs (TpF-COFs) by adjusting the proportion of fluorine containing functional groups on TpH-COF and TpS-COF according to the theoretical calculations. the obtained adsorption energies of all Li_2S_x species on TpS are much higher than those on TpH counterparts, which originates from the additional adsorption effect of bonded C-S on Li_2S_x besides the carbonyl groups [149].

Based on the band structures and PDOS plots of TpH and TpS, both materials exhibit semiconductor properties, band gaps are 1.8 eV and 1.1 eV respectively, revealing their excellent electronic conductivity for S-LIBs applications, especially TpS [149].

3.4 Modeling and simulation of COF-based electrolytes

A perfect conductor must possess an appropriate channel size to exclusively facilitate Li^+ ion conduction. It should also maintain an optimal concentration of vacant and interstitial spots, possess a low energy barrier for ion diffusion, and exhibit chemical and electrochemical stability when faced with electrode interfaces [104].

In 2013, Kecheng Zhang utilized AIMD simulation to analyze the dynamics and microstructural Research in the field of LIBs has predominantly concentrated on liquid electrolytes. While liquid electrolytes can offer advantages such as high ionic conductivity and easy accessibility, they frequently encounter issues with electrochemical and thermal stabilities, as well as limited ion-selectivity. Additionally, their liquid form raises concerns regarding volatilization, flammability, and the potential for explosions [150]. In 1992, the solid-state electrolyte known as lithium phosphorus oxynitride (LiPON) was introduced for the first time [151, 152]. Solid-state electrolytes are typically divided into two categories based on their carriers: solid inorganic ceramic electrolytes (SIE) and solid polymer electrolytes (SPE). COFs with open channels have been reported as solid-state electrolytes. Several groups of COFs are introduced as electrolytes for LIBs including ionic COFs (ICOFs) [153, 154], Crystalline COFs [155, 156] and 2D COFs [157, 158].

Kecheng Zhang et al performed AIMD simulation to investigate changes that occur during the diffusion of Li^+ ions in a 2D-COF based electrolyte composed of COF-5, $LiClO_4$ and tetrahydrofuran (THF). The mean square displacement (MSD, denoted by $\langle \boldsymbol{r} \rangle^2 = \boldsymbol{6Dt}$ [159]) of Li^+ ions as a function of time ($\boldsymbol{t}$) calculated by AIMD simulation at 300 K shows that the linear dependence of MSD; that is, Li ions will not simply oscillate inside the O_4 cages but instead exhibit diffusive behavior at room temperature. the probability density of Li^+ ions at 700 K [160] indicates that Li^+ diffusion is mainly confined in the middle region of the tunnels, implying that Li^+ ions are reluctant to approach the COF-5 framework [161].

Kihun Jeong and colleagues [162] introduced a novel type of solvent-free, single Li-ion conductors in the form of a lithium sulfonated COF, referred to as TpPa-SO_3Li. The TpPa-SO_3Li exhibited aporous crystalline structure, where the hydrogen atoms of sulfonic acids were replaced by Li atoms. The stable locations of these Li atoms were determined through geometry optimization using a 1×1×2 supercell model with 336 atoms. The PXRD pattern exhibits distinct diffraction peaks at $2\theta = 4.6$ and 26.2 degrees, corresponding to the (100) and (001) planes, respectively. These peaks bear a striking resemblance to the simulated pattern derived from the structural model. The theoretical findings confirm the directional conduction of Li-ion along the stacked pores of TpPa-SO_3Li, where the keto group's O atoms have a significant role to play [162] A range of single-ion conducting imidazolate ICOFs (Li-ImCOFs) were created and produced by Yiming Hu, showcasing remarkable lithium-ion conductivity at room temperature, reaching up to 7.2×10^{-3} S cm^{-1}. These ICOFs also possess a low activation energy as low as 0.10 eV and a high transference number of 0.81. DFT is employed to calculate the pore size distribution of H-ImCOF and H-Li-ImCOF. The results obtained from the cylindrical pore model exhibit a good agreement with the quenched solid density functional theory (QSDFT) analysis. Furthermore, the simulated

PXRD patterns exhibit a strong correlation with the experimental findings [163].

4. Conclusion

This review provided insights into the principles of modeling lithium batteries and delineated specific computational techniques for simulating COF-integrated components. By exploring COF-based LIB's advantages and potential challenges, we have investigated the significance of theoretical modeling and simulation methods in unraveling the complexities of COF-based battery systems. Understanding and mitigating the challenges associated with COF integration-such as structural stability and conductivity-will drive research toward tailored COF designs and improved modeling approaches. Moreover, the optimization of COF-based anodes, cathodes, electrolytes, and separators presents opportunities to enhance key performance parameters like capacity, energy density, cycle life, and safety. As the field progresses, emerging technologies significantly impact COF-based lithium batteries. Innovations in solid-state electrolytes, sustainable materials, and advancements in nanotechnology offer potential breakthroughs. Additionally, the integration of machine learning and artificial intelligence could revolutionize battery design and optimization. By leveraging theoretical insights and computational methods, the pursuit of optimized COF-based lithium batteries remains poised to revolutionize energy storage, paving the way for more efficient and sustainable solutions in the near future.

5. Reference

1. Abbasi KR, Adedoyin FF, Abbas J, Hussain K, The impact of energy depletion and renewable energy on CO2 emissions in Thailand: fresh evidence from the novel dynamic ARDL simulation, Renewable Energy, 1439-1450, 180(2021)
2. Furlan C, Mortarino C, Forecasting the impact of renewable energies in competition with non-renewable sources, Renewable and Sustainable Energy Reviews, 1879-1886, 81(2018)
3. Diouf B, Pode R, Potential of lithium-ion batteries in renewable energy, Renewable Energy, 375-380, 76(2015)
4. Yang J, Hu C, Wang H, Yang K, Liu JB, Yan H, Review on the research of failure modes and mechanism for lead–acid batteries, International Journal of Energy Research, 336-352, 41(2017)
5. Nayak PK, Yang L, Brehm W, Adelhelm P, From lithium-ion to sodium-ion batteries: advantages, challenges, and surprises, Angewandte Chemie International Edition, 102-120, 57(2018)
6. Ghafari A, Bayat V, Akbari S, Yeklangi AG, Current and future prospects of Li-ion batteries: a review, NanoSci Technol, 24-43, 8(2023)
7. Ghafari A, Mohammadi E, Dastjerdi M, Honarmand S, Radmoghadam ZA, Akbari S, Batteries applications in the biomedical industry: A review, (2023)
8. Jeyaseelan C, Jain A, Khurana P, Kumar D, Thatai S, Ni-Cd Batteries, Rechargeable Batteries: History, Progress, and Applications, 177-194, (2020)
9. Schon TB, McAllister BT, Li P-F, Seferos DS, The rise of organic electrode materials for energy storage, Chemical Society Reviews, 6345-6404, 45(2016)
10. O'Keeffe M, Design of MOFs and intellectual content in reticular chemistry: a personal view, Chemical Society Reviews, 1215-1217, 38(2009)
11. Feng X, Ding X, Jiang D, Covalent organic frameworks, Chemical Society Reviews, 6010-6022, 41(2012)
12. Jia M, Zhang L, Yuan Q, Application of New COF Materials in Secondary Battery Anode Materials, Molecules, 5953, 28(2023)
13. Cote AP, Benin AI, Ockwig NW, O'Keeffe M, Matzger AJ, Yaghi OM, Porous, crystalline, covalent organic frameworks, science, 1166-1170, 310(2005)
14. Zhao X, Pachfule P, Thomas A, Covalent organic frameworks (COFs) for electrochemical applications, Chemical Society Reviews, 6871-6913, 50(2021)
15. Wu M-X, Yang Y-W, Applications of covalent organic frameworks (COFs): From gas storage and separation to drug delivery, Chinese Chemical Letters, 1135-1143, 28(2017)
16. Bayat V, Ghafari A, Asgari F, Radmoghaddam ZA, Yeklangi AG, Akbari S, Covalent organic frameworks for next-generation of lithium-ion batteries, NanoSci Technol, 1-23, 8(2023)
17. Ghafari A, Yeklangi AG, Sima FA, Akbari S, Industrial-scale synthesis and application of covalent organic frameworks in lithium battery technology, Journal of Applied Electrochemistry, 215-243, 54(2024)

18. Nitta N, Wu F, Lee JT, Yushin G, Li-ion battery materials: present and future, Materials today, 252-264, 18(2015)
19. Chen Z, Zhang W, Yang Z, A review on cathode materials for advanced lithium ion batteries: microstructure designs and performance regulations, Nanotechnology, 012001, 31(2019)
20. Manthiram A, A reflection on lithium-ion battery cathode chemistry, Nature communications, 1550, 11(2020)
21. Kucinskis G, Bajars G, Kleperis J, Graphene in lithium ion battery cathode materials: A review, Journal of Power Sources, 66-79, 240(2013)
22. Xu F, Jin S, Zhong H, Wu D, Yang X, Chen X, Wei H, Fu R, Jiang D, Electrochemically active, crystalline, mesoporous covalent organic frameworks on carbon nanotubes for synergistic lithium-ion battery energy storage, Scientific Reports, 8225, 5(2015)
23. Luo Z, Liu L, Ning J, Lei K, Lu Y, Li F, Chen J, A microporous covalent–organic framework with abundant accessible carbonyl groups for lithium-ion batteries, Angewandte Chemie International Edition, 9443-9446, 57(2018)
24. Yang D-H, Yao Z-Q, Wu D, Zhang Y-H, Zhou Z, Bu X-H, Structure-modulated crystalline covalent organic frameworks as high-rate cathodes for Li-ion batteries, Journal of Materials Chemistry A, 18621-18627, 4(2016)
25. Fang Q, Zhuang Z, Gu S, Kaspar RB, Zheng J, Wang J, Qiu S, Yan Y, Designed synthesis of large-pore crystalline polyimide covalent organic frameworks, Nature communications, 4503, 5(2014)
26. Fang Q, Wang J, Gu S, Kaspar RB, Zhuang Z, Zheng J, Guo H, Qiu S, Yan Y, 3D porous crystalline polyimide covalent organic frameworks for drug delivery, Journal of the American chemical society, 8352-8355, 137(2015)
27. Li X, Wang H, Chen Z, Xu HS, Yu W, Liu C, Wang X, Zhang K, Xie K, Loh KP, Covalent-organic-framework-based Li–CO2 batteries, Advanced Materials, 1905879, 31(2019)
28. He J, Bhargav A, Manthiram A, Covalent Organic Framework as an Efficient Protection Layer for a Stable Lithium-Metal Anode, Angewandte Chemie, e202116586, 134(2022)
29. Gao C, Jiang Z, Qi S, Wang P, Jensen LR, Johansen M, Christensen CK, Zhang Y, Ravnsbæk DB, Yue Y, Metal-organic framework glass anode with an exceptional cycling-induced capacity enhancement for lithium-ion batteries, Advanced Materials, 2110048, 34(2022)
30. Li Z, Liu Z-W, Mu Z-J, Cao C, Li Z, Wang T-X, Li Y, Ding X, Han B-H, Feng W, Cationic covalent organic framework based all-solid-state electrolytes, Materials Chemistry Frontiers, 1164-1173, 4(2020)
31. Santiago-Maldonado X: Covalent− organic framework-based electrolytes fabricated for solid-state Li-ion batteries. In.: Springer; 2021.
32. Shan Z, Wu M, Du Y, Xu B, He B, Wu X, Zhang G, Covalent organic framework-based electrolytes for fast Li+ conduction and high-temperature solid-state lithium-ion batteries, Chemistry of Materials, 5058-5066, 33(2021)
33. Luiso S, Fedkiw P, Lithium-ion battery separators: Recent developments and state of art, Current Opinion in Electrochemistry, 99-107, 20(2020)
34. Wen Y, Wang X, Yang Y, Liu M, Tu W, Xu M, Sun G, Kawaguchi S, Cao G, Li W, Covalent organic framework-regulated ionic transportation for high-performance lithium-ion batteries, Journal of Materials Chemistry A, 26540-26548, 7(2019)
35. Sun T, Xie J, Guo W, Li DS, Zhang Q, Covalent–organic frameworks: advanced organic electrode materials for rechargeable batteries, Advanced Energy Materials, 1904199, 10(2020)
36. Pallasch S, Bhosale M, Smales GJ, Schmidt C, Riedel S, Zhao-Karger Z, Esser B, Dumele O, A Porous Azatruxene Covalent Organic Framework as Positive Electrode Materials in Li-and Mg-based Batteries, (2023)
37. Wu M, Zhao Y, Zhang H, Zhu J, Ma Y, Li C, Zhang Y, Chen Y, A 2D covalent organic framework with ultra-large interlayer distance as high-rate anode material for lithium-ion batteries, Nano Research, 9779-9784, 15(2022)
38. Khurram Tufail M, Ahmed A, Rafiq M, Asif Nawaz M, Shoaib Ahmad Shah S, Sohail M, Sufyan Javed M, Najam T, Althomali RH, Rahman MM, Chemistry Aspects and Designing Strategies of Flexible Materials for High-Performance Flexible Lithium-Ion Batteries, The Chemical Record, e202300155, (2023)
39. Wang X-X, Chi X-W, Li M-L, Guan D-H, Miao C-L, Xu J-J, An integrated solid-state lithium-oxygen battery with highly stable anionic covalent organic frameworks electrolyte, Chem, 394-410, 9(2023)
40. Wang Z, Hu J, Lu Z, Covalent Organic Frameworks as Emerging Battery Materials, Batteries & Supercaps, e202200545, 6(2023)
41. Heidari M, Solimannejad M, A DFT study of COF-1 covalent organic framework as a disposable platform for rechargeable lithium-ion battery

anodes, Physica B: Condensed Matter, 415027, (2023)
42. Jindal P, Sharma P, Kundu M, Singh S, Shukla DK, Pawar VJ, Wei Y, Breedon P, Computational Fluid Dynamics (CFD) analysis of Graphene Nanoplatelets for the cooling of a multiple tier Li-ion battery pack, Thermal Science and Engineering Progress, 101282, 31(2022)
43. Li W, Garg A, Wang N, Gao L, Le Phung ML, Tran VM, Computational fluid dynamics-based numerical analysis for studying the effect of mini-channel cooling plate, flow characteristics, and battery arrangement for cylindrical lithium-ion battery pack, Journal of Electrochemical Energy Conversion and Storage, 041003, 19(2022)
44. Choi W, Shin H-C, Kim JM, Choi J-Y, Yoon W-S, Modeling and applications of electrochemical impedance spectroscopy (EIS) for lithium-ion batteries, Journal of Electrochemical Science and Technology, 1-13, 11(2020)
45. Guo D, Ming F, Shinde DB, Cao L, Huang G, Li C, Li Z, Yuan Y, Hedhili MN, Alshareef HN, Covalent assembly of two-dimensional COF-on-MXene heterostructures enables fast charging lithium hosts, Advanced Functional Materials, 2101194, 31(2021)
46. Zhai P, Liu K, Wang Z, Shi L, Yuan S, Multifunctional separators for high-performance lithium ion batteries, Journal of Power Sources, 229973, 499(2021)
47. Zhang X, Li Z, Luo L, Fan Y, Du Z, A review on thermal management of lithium-ion batteries for electric vehicles, Energy, 121652, 238(2022)
48. Zhao J, Ling H, Liu J, Wang J, Burke AF, Lian Y, Machine learning for predicting battery capacity for electric vehicles, ETransportation, 100214, 15(2023)
49. Kaleem MB, He W, Li H, Machine learning driven digital twin model of Li-ion batteries in electric vehicles: a review, Artif Intell Auton Syst, 0003, 1(2023)
50. Zhao X, Callafon RAd, Modeling of battery dynamics and hysteresis for power delivery prediction and SOC estimation, Applied Energy, 823-833, 180(2016)
51. Dineva AA, Kocsis SS, Vajda I, Data-driven Terminal Voltage Prediction of Li-ion Batteries Under Dynamic Loads, 2020 21st International Symposium on Electrical Apparatus & Technologies (SIELA), 1-5, (2020)
52. He Q, Yu B, Li Z, Zhao Y, Density Functional Theory for Battery Materials, ENERGY & ENVIRONMENTAL MATERIALS, 264-279, 2(2019)
53. Li AG, Preindl M: Modelling the Diffusion Overpotential in Li-ion Batteries using a State-Space System with Receding Horizon. In*: 2022*.
54. Kim K, Choi Y-J, Kim H, Data-driven battery degradation model leveraging average degradation function fitting, Electronics Letters, 102-104, 53(2017)
55. Allam O, Cho BW, Kim KC, Jang SS, Application of DFT-based machine learning for developing molecular electrode materials in Li-ion batteries, RSC Advances, 39414 - 39420, 8(2018)
56. Wang Y, Yu B, Xiao J, Zhou L, Chen M, Application of First Principles Computations Based on Density Functional Theory (DFT) in Cathode Materials of Sodium-Ion Batteries, Batteries, (2023)
57. Wu J, Ihsan-Ul-Haq M, Chen Y, Kim JK, Understanding solid electrolyte interphases: Advanced characterization techniques and theoretical simulations, Nano Energy, (2021)
58. Born M, Oppenheimer R, Zur Quantentheorie der Molekeln Annalen der Physik, v. 84, (1927)
59. Guest M, Saunders V, On methods for converging open-shell Hartree-Fock wave-functions, Molecular Physics, 819-828, 28(1974)
60. Wu X, Kang F, Duan W, Li J, Density functional theory calculations: A powerful tool to simulate and design high-performance energy storage and conversion materials, Progress in Natural Science: Materials International, 247-255, 29(2019)
61. Hohenberg P, Kohn W, Inhomogeneous electron gas, Physical review, B864, 136(1964)
62. Kohn W, Sham LJ, Self-consistent equations including exchange and correlation effects, Physical review, A1133, 140(1965)
63. Meutzner F, Nestler T, Zschornak M, Canepa P, Gautam GS, Leoni S, Adams S, Leisegang T, Blatov VA, Meyer DC, Computational analysis and identification of battery materials, Physical Sciences Reviews, 4(2018)
64. Sun Y, Yang T, Ji H, Zhou J, Wang Z, Qian T, Yan C, Boosting the Optimization of Lithium Metal Batteries by Molecular Dynamics Simulations: A Perspective, Advanced Energy Materials, 10(2020)
65. Walker WQ, Ardebili H, Thermo-electrochemical analysis of lithium ion batteries for space applications using Thermal Desktop, Journal of Power Sources, 486-497, 269(2014)
66. Fallahzadeh R, Farhadian N, Molecular dynamics simulation of lithium ion diffusion in LiCoO2

cathode material, Solid State Ionics, 10-17, 280(2015)
67. Hofmann T, Müller R, Andrä H, Zausch J, Numerical simulation of phase separation in cathode materials of lithium ion batteries, International Journal of Solids and Structures, 456-469, 100(2016)
68. Tahmasbi AA, Eikerling MH, Statistical physics-based model of mechanical degradation in lithium ion batteries, Electrochimica Acta, (2018)
69. Li J, Cheng Y, Li-hua A, Jia M, Du S, Baohua Y, Woo SW, Zhang H-l, 3D simulation on the internal distributed properties of lithium-ion battery with planar tabbed configuration, Journal of Power Sources, 993-1005, 293(2015)
70. Grigera J, Molecular dynamics simulation for ligand-receptor studies. Carbohydrates interactions in aqueous solutions, Current pharmaceutical design, 1579-1604, 8(2002)
71. Martyna GJ, Tobias DJ, Klein ML, Constant pressure molecular dynamics algorithms, The Journal of chemical physics, 4177-4189, 101(1994)
72. Nichols RJ, Molecular electronics at electrode–electrolyte interfaces, Current Opinion in Electrochemistry, 100650, 25(2021)
73. Ponce V, Galvez-Aranda DE, Seminario JM, Analysis of a Li-Ion Nanobattery with Graphite Anode Using Molecular Dynamics Simulations, Journal of Physical Chemistry C, 12959-12971, 121(2017)
74. Rodrigues M-TF, Kalaga K, Trask SE, Dees DW, Shkrob IA, Abraham DP, Fast Charging of Li-Ion Cells: Part I. Using Li/Cu Reference Electrodes to Probe Individual Electrode Potentials, Journal of The Electrochemical Society, (2019)
75. Wang Z, VahidMohammadi A, Ouyang L, Erlandsson J, Tai CW, Wågberg L, Hamedi MM, Layer-by-Layer Self-Assembled Nanostructured Electrodes for Lithium-Ion Batteries, Small, e2006434, (2020)
76. Zhang G, Wang H, Deng X, Yang Y, Zhang T, Wang J, Zeng H, Wang C, Deng Y, Metal chelation based supramolecular self-assembly enables a high-performance organic anode for lithium ion batteries, Chemical Engineering Journal, 127525, (2020)
77. Roux FAl, Bergveld HJ, Donkers MCF, Improved Parameter Estimation of the Doyle-Fuller-Newman Model by Incorporating Temperature Dependence, IFAC-PapersOnLine, 6136-6141, 56(2023)
78. Khalik Z, Donkers MCF, Sturm J, Bergveld HJ, Parameter estimation of the Doyle–Fuller–Newman model for Lithium-ion batteries by parameter normalization, grouping, and sensitivity analysis, Journal of Power Sources, 229901, 499(2021)
79. Wang J, Meng J, Peng Q, Liu T, Zeng X, Chen G, Li Y, Lithium-Ion Battery State-of-Charge Estimation Using Electrochemical Model with Sensitive Parameters Adjustment, Batteries, 180, 9(2023)
80. Wang D, Gao Y, Zhang X, Dong T, Zhu C: A novel pseudo two-dimensional model for NCM Liion battery based on electrochemical-thermal coupling analysis. In: *2020 3rd International Conference on Electron Device and Mechanical Engineering (ICEDME): 1-3 May 2020 2020*. 110-116.
81. Xue C, Jiang B, Zhu J, Wei X, Dai H, An Enhanced Single-Particle Model Using a Physics-Informed Neural Network Considering Electrolyte Dynamics for Lithium-Ion Batteries, Batteries, 511, 9(2023)
82. Ríos-Alborés A, Rodríguez J: Single Particle Models for the Numerical Simulation of Lithium-Ion Cells. In: *Advances on Links Between Mathematics and Industry: 2021// 2021; Cham*. Springer International Publishing: 91-106.
83. Cui X, Zeng J, Zhang H, Yang J, Qiao J, Li J, Li W, Optimization of the lumped parameter thermal model for hard-cased li-ion batteries, Journal of Energy Storage, 101758, 32(2020)
84. Dey S, Perez HE, Moura SJ: Thermal fault diagnostics in Lithium-ion batteries based on a distributed parameter thermal model. In: *2017 American Control Conference (ACC): 24-26 May 2017 2017*. 68-73.
85. Lin X, Perez HE, Mohan S, Siegel JB, Stefanopoulou AG, Ding Y, Castanier MP, A lumped-parameter electro-thermal model for cylindrical batteries, Journal of Power Sources, 1-11, 257(2014)
86. Zhu D, Xu G, Barnes M, Li Y, Tseng CP, Zhang Z, Zhang JJ, Zhu Y, Khalil S, Rahman MM, Covalent organic frameworks for batteries, Advanced Functional Materials, 2100505, 31(2021)
87. Xie Y, Zhang T, Chen Y, Wang Y, Wang L, Fabrication of core-shell magnetic covalent organic frameworks composites and their application for highly sensitive detection of luteolin, Talanta, 120843, 213(2020)
88. Lu Z, Wang Y, Li G, Covalent Organic Frameworks-Based Electrochemical Sensors for Food Safety Analysis, Biosensors, 291, 13(2023)
89. Berthier C, Gorecki W, Minier M, Armand M, Chabagno J, Rigaud P, Microscopic investigation of ionic conductivity in alkali metal salts-poly

(ethylene oxide) adducts, Solid State Ionics, 91-95, 11(1983)
90. Wang A, Tan R, Breakwell C, Wei X, Fan Z, Ye C, Malpass-Evans R, Liu T, Zwijnenburg MA, Jelfs KE, Solution-processable redox-active polymers of intrinsic microporosity for electrochemical energy storage, Journal of the American Chemical Society, 17198-17208, 144(2022)
91. Meng Y, Lin G, Ding H, Liao H, Wang C, Impregnation of sulfur into a 2D pyrene-based covalent organic framework for high-rate lithium–sulfur batteries, Journal of Materials Chemistry A, 17186-17191, 6(2018)
92. Elgrishi N, Rountree KJ, McCarthy BD, Rountree ES, Eisenhart TT, Dempsey JL, A practical beginner's guide to cyclic voltammetry, Journal of chemical education, 197-206, 95(2018)
93. Irvine JT, Sinclair DC, West AR, Electroceramics: characterization by impedance spectroscopy, Advanced materials, 132-138, 2(1990)
94. Wang S, Zhang J, Gharbi O, Vivier V, Gao M, Orazem ME, Electrochemical impedance spectroscopy, Nature Reviews Methods Primers, 41, 1(2021)
95. Elanthamilan E, Rajkumar S, Rajavalli R, Merlin JP, Cost effective synthesis of a copper-1 H-imidazole@ activated carbon metal organic framework as an electrode material for supercapacitor applications, New Journal of Chemistry, 10300-10308, 42(2018)
96. Vadhva P, Hu J, Johnson MJ, Stocker R, Braglia M, Brett DJ, Rettie AJ, Electrochemical impedance spectroscopy for all-solid-state batteries: Theory, methods and future outlook, ChemElectroChem, 1930-1947, 8(2021)
97. Ai Q, Fang Q, Liang J, Xu X, Zhai T, Gao G, Guo H, Han G, Ci L, Lou J, Lithium-conducting covalent-organic-frameworks as artificial solid-electrolyte-interphase on silicon anode for high performance lithium ion batteries, Nano Energy, 104657, 72(2020)
98. Chen L, Li Y, Chen L, Li N, Dong C, Chen Q, Liu B, Ai Q, Si P, Feng J, A large-area free-standing graphene oxide multilayer membrane with high stability for nanofiltration applications, Chemical Engineering Journal, 536-544, 345(2018)
99. Zhang Y, Wu Y, An Y, Wei C, Tan L, Xi B, Xiong S, Feng J, Ultrastable and High-Rate 2D Siloxene Anode Enabled by Covalent Organic Framework Engineering for Advanced Lithium-Ion Batteries, Small Methods, 2200306, 6(2022)
100. Heist A, Lee S-H, Electrochemical Analysis of Factors Affecting the Kinetic Capabilities of an Ionic Liquid Electrolyte, Journal of The Electrochemical Society, A1677, 166(2019)
101. Talaie E, Bonnick P, Sun X, Pang Q, Liang X, Nazar LF, Methods and protocols for electrochemical energy storage materials research, Chemistry of Materials, 90-105, 29(2017)
102. Smith A, Burns J, Trussler S, Dahn J, Precision measurements of the coulombic efficiency of lithium-ion batteries and of electrode materials for lithium-ion batteries, Journal of The Electrochemical Society, A196, 157(2009)
103. Huggins R: Advanced batteries: materials science aspects: Springer Science & Business Media; 2008.
104. Angell C, Mobile ions in amorphous solids, Annual review of physical chemistry, 693-717, 43(1992)
105. Xuan W, Ramachandran R, Zhao C, Wang F, Influence of synthesis temperature on cobalt metal-organic framework (Co-MOF) formation and its electrochemical performance towards supercapacitor electrodes, Journal of Solid State Electrochemistry, 3873-3881, 22(2018)
106. Wu J, Rui X, Wang C, Pei WB, Lau R, Yan Q, Zhang Q, Nanostructured conjugated ladder polymers for stable and fast lithium storage anodes with high-capacity, Advanced Energy Materials, 1402189, 5(2015)
107. Fäßler F, Javoor MG, Datler J, Döring H, Hofer FW, Dimchev G, Hodirnau V-V, Faix J, Rottner K, Schur FK, ArpC5 isoforms regulate Arp2/3 complex-dependent protrusion through differential Ena/VASP positioning, Science Advances, eadd6495, 9(2023)
108. Du J, Sun Q, He W, Liu L, Song Z, Yao A, Ma J, Cao D, Hassan SU, Guan J, A 2D soft covalent organic framework membrane prepared via a molecular bridge, Advanced Materials, 2300975, 35(2023)
109. Shi X, Zhang Z, Yin C, Zhang X, Long J, Zhang Z, Wang Y, Design of Three-Dimensional Covalent Organic Framework Membranes for Fast and Robust Organic Solvent Nanofiltration, Angewandte Chemie International Edition, e202207559, 61(2022)
110. Dautzenberg E, Lam M, Li G, de Smet LC, Enhanced surface area and reduced pore collapse of methylated, imine-linked covalent organic frameworks, Nanoscale, 19446-19452, 13(2021)
111. Wang D-G, Qiu T, Guo W, Liang Z, Tabassum H, Xia D, Zou R, Covalent organic framework-based

materials for energy applications, Energy & Environmental Science, 688-728, 14(2021)
112. Hu J, Gupta SK, Ozdemir J, Beyzavi H, Applications of dynamic covalent chemistry concept toward tailored covalent organic framework nanomaterials: A review, ACS applied nano materials, 6239-6269, 3(2020)
113. Hu S, Wu P, Cao W, Liu J, Tang X: VASP porting and parallel optimization on GPU like accelerator. In: *3rd International Conference on Applied Mathematics, Modelling, and Intelligent Computing (CAMMIC 2023): 2023*. SPIE: 601-607.
114. Fang L, Cao X, Cao Z, Covalent organic framework with high capacity for the lithium ion battery anode: insight into intercalation of Li from first-principles calculations, Journal of Physics: Condensed Matter, 205502, 31(2019)
115. Laxmi D, Priyadarshy S, HyperChem 6.03, Biotech Software & Internet Report: The Computer Software Journal for Scientists, 5-9, 3(2002)
116. Paredes-Doig A, Pinedo-Flores A, Aylas-Orejón J, Obregón-Valencia D, Sun Kou M, The interaction of metallic ions onto activated carbon surface using computational chemistry software, Adsorption Science & Technology, 191-204, 38(2020)
117. Rosli A, Stephen Paul SA, Low SC, Computational analysis of atomic binding energy for organosilicon-low-density polyethylene-coated silica embedded in polyvinylidene fluoride composite membrane for membrane gas absorption, International Journal of Energy Research, 15372-15388, 45(2021)
118. Sabet R, Jafroudi I, QSAR, Docking Study of Isatin Analogues as Anti-bacterial Agents for Design New Compounds, Journal of Pharmaceutical Research International, 1-24, 31(2019)
119. Streif M, Neukart F, Leib M: Solving quantum chemistry problems with a d-wave quantum annealer. In: *Quantum Technology and Optimization Problems: First International Workshop, QTOP 2019, Munich, Germany, March 18, 2019, Proceedings 1: 2019*. Springer: 111-122.
120. Zhao J, Zhou M, Chen J, Tao L, Zhang Q, Li Z, Zhong S, Fu H, Wang H, Wu L, Phthalocyanine-based covalent organic frameworks as novel anode materials for high-performance lithium-ion/sodium-ion batteries, Chemical Engineering Journal, 131630, 425(2021)
121. Mohamed N, Allam NK, Recent advances in the design of cathode materials for Li-ion batteries, RSC advances, 21662-21685, 10(2020)
122. Mizushima K, Jones P, Wiseman P, Goodenough JB, LixCoO2 (0< x<-1): A new cathode material for batteries of high energy density, Materials Research Bulletin, 783-789, 15(1980)
123. Kim U-H, Jun D-W, Park K-J, Zhang Q, Kaghazchi P, Aurbach D, Major DT, Goobes G, Dixit M, Leifer N, Pushing the limit of layered transition metal oxide cathodes for high-energy density rechargeable Li ion batteries, Energy & environmental science, 1271-1279, 11(2018)
124. Li W, Song B, Manthiram A, High-voltage positive electrode materials for lithium-ion batteries, Chemical Society Reviews, 3006-3059, 46(2017)
125. Kong D, Hu J, Chen Z, Song K, Li C, Weng M, Li M, Wang R, Liu T, Liu J, Ti-Gradient doping to stabilize layered surface structure for high performance high-Ni oxide cathode of Li-ion battery, Advanced Energy Materials, 1901756, 9(2019)
126. Yu H, Cao Y, Chen L, Hu Y, Duan X, Dai S, Li C, Jiang H, Surface enrichment and diffusion enabling gradient-doping and coating of Ni-rich cathode toward Li-ion batteries, Nature Communications, 4564, 12(2021)
127. Zhang J-N, Li Q, Ouyang C, Yu X, Ge M, Huang X, Hu E, Ma C, Li S, Xiao R, Trace doping of multiple elements enables stable battery cycling of LiCoO2 at 4.6 V, Nature Energy, 594-603, 4(2019)
128. He W, Ye F, Lin J, Wang Q, Xie Q, Pei F, Zhang C, Liu P, Li X, Wang L, Boosting the electrochemical performance of Li-and Mn-rich cathodes by a three-in-one strategy, Nano-Micro Letters, 1-11, 13(2021)
129. Paulsen J, Thomas C, Dahn J, Layered Li-Mn-oxide with the O2 structure: a cathode material for Li-ion cells which does not convert to spinel, Journal of the Electrochemical Society, 3560, 146(1999)
130. Armstrong AR, Bruce PG, Synthesis of layered LiMnO2 as an electrode for rechargeable lithium batteries, Nature, 499-500, 381(1996)
131. Sun H-H, Manthiram A, Impact of microcrack generation and surface degradation on a nickel-rich layered Li [Ni0. 9Co0. 05Mn0. 05] O2 cathode for lithium-ion batteries, Chemistry of materials, 8486-8493, 29(2017)
132. Xie J, Gu P, Zhang Q, Nanostructured conjugated polymers: toward high-performance organic electrodes for rechargeable batteries, ACS Energy Letters, 1985-1996, 2(2017)
133. Liang Y, Tao Z, Chen J, Organic electrode materials for rechargeable lithium batteries, Advanced Energy Materials, 742-769, 2(2012)

134. Muench S, Wild A, Friebe C, Haupler B, Janoschka T, Schubert US, Polymer-based organic batteries, Chemical reviews, 9438-9484, 116(2016)
135. Zeng S-m, Huang X-x, Ma Y-j, Zhi L-j, A review of covalent organic framework electrode materials for rechargeable metal-ion batteries, New Carbon Materials, 1-18, 36(2021)
136. Wu M, Zhou Z, Covalent organic frameworks as electrode materials for rechargeable metal-ion batteries, Interdisciplinary Materials, 231-259, 2(2023)
137. AlHazaimeh T, Raheem M, Al-Othman A, Covalent Organic Frameworks (COFs): Characteristics and Applications for Lithium-Ion Batteries (LIBs) and Sodium Ion Batteries (SIBs), International Journal of Thermofluids, 100531, 21(2024)
138. Yoo J, Cho S-J, Jung GY, Kim SH, Choi K-H, Kim J-H, Lee CK, Kwak SK, Lee S-Y, COF-Net on CNT-Net as a Molecularly Designed, Hierarchical Porous Chemical Trap for Polysulfides in Lithium–Sulfur Batteries, Nano Letters, 3292-3300, 16(2016)
139. Xiao Z, Li L, Tang Y, Cheng Z, Pan H, Tian D, Wang R, Covalent organic frameworks with lithiophilic and sulfiphilic dual linkages for cooperative affinity to polysulfides in lithium-sulfur batteries, Energy Storage Materials, 252-259, 12(2018)
140. Li B-Q, Zhang S-Y, Wang B, Xia Z-J, Tang C, Zhang Q, A porphyrin covalent organic framework cathode for flexible Zn–air batteries, Energy & Environmental Science, 1723-1729, 11(2018)
141. Wang S, Wang Q, Shao P, Han Y, Gao X, Ma L, Yuan S, Ma X, Zhou J, Feng X, Exfoliation of covalent organic frameworks into few-layer redox-active nanosheets as cathode materials for lithium-ion batteries, Journal of the American Chemical Society, 4258-4261, 139(2017)
142. Khayum M A, Vijayakumar V, Karak S, Kandambeth S, Bhadra M, Suresh K, Acharambath N, Kurungot S, Banerjee R, Convergent covalent organic framework thin sheets as flexible supercapacitor electrodes, ACS applied materials & interfaces, 28139-28146, 10(2018)
143. Zhan X, Chen Z, Zhang Q, Recent progress in two-dimensional COFs for energy-related applications, Journal of Materials Chemistry A, 14463-14479, 5(2017)
144. Kim G, Yang J, Nakashima N, Shiraki T, Highly microporous nitrogen-doped carbon synthesized from azine-linked covalent organic framework and its supercapacitor function, Chemistry–A European Journal, 17504-17510, 23(2017)
145. Ghazi ZA, Zhu L, Wang H, Naeem A, Khattak AM, Liang B, Khan NA, Wei Z, Li L, Tang Z, Efficient polysulfide chemisorption in covalent organic frameworks for high-performance lithium-sulfur batteries, Advanced Energy Materials, 1601250, 6(2016)
146. Gomes R, Bhattacharyya AJ, Carbon nanotube-templated covalent organic framework nanosheets as an efficient sulfur host for room-temperature metal–sulfur batteries, ACS Sustainable Chemistry & Engineering, 5946-5953, 8(2020)
147. Jiang G, Xu F, Yang S, Wu J, Wei B, Wang H, Mesoporous, conductive molybdenum nitride as efficient sulfur hosts for high-performance lithium-sulfur batteries, Journal of Power Sources, 77-84, 395(2018)
148. Xu F, Yang S, Chen X, Liu Q, Li H, Wang H, Wei B, Jiang D, Energy-storage covalent organic frameworks: improving performance via engineering polysulfide chains on walls, Chemical science, 6001-6006, 10(2019)
149. Qiu T, Tang W, Han X, Li Y, Chen Z, Yao R, Li Y, Wang Y, Li Y, Tan H, Fluorine/sulfur-comodulated covalent organic frameworks cathode for high-performance lithium ion batteries, Chemical Engineering Journal, 143149, 466(2023)
150. Quartarone E, Mustarelli P, Electrolytes for solid-state lithium rechargeable batteries: recent advances and perspectives, Chemical Society Reviews, 2525-2540, 40(2011)
151. Dudney N, Bates J, Zuhr R, Luck C, Robertson J, Sputtering of lithium compounds for preparation of electrolyte thin films, solid state ionics, 655-661, 53(1992)
152. Bates J, Dudney N, Gruzalski G, Zuhr R, Choudhury A, Luck C, Robertson J, Electrical properties of amorphous lithium electrolyte thin films, Solid state ionics, 647-654, 53(1992)
153. Zhang Y, Duan J, Ma D, Li P, Li S, Li H, Zhou J, Ma X, Feng X, Wang B, Three-dimensional anionic cyclodextrin-based covalent organic frameworks, Angewandte Chemie International Edition, 16313-16317, 56(2017)
154. Du Y, Yang H, Whiteley JM, Wan S, Jin Y, Lee SH, Zhang W, Ionic covalent organic frameworks with spiroborate linkage, Angewandte Chemie International Edition, 1737-1741, 55(2016)
155. Gadjourova Z, Andreev YG, Tunstall DP, Bruce PG, Ionic conductivity in crystalline polymer electrolytes, Nature, 520-523, 412(2001)

156. Stoeva Z, Martin-Litas I, Staunton E, Andreev YG, Bruce PG, Ionic conductivity in the crystalline polymer electrolytes PEO6: LiXF6, X= P, As, Sb, Journal of the American Chemical Society, 4619-4626, 125(2003)
157. Vazquez-Molina DA, Mohammad-Pour GS, Lee C, Logan MW, Duan X, Harper JK, Uribe-Romo FJ, Mechanically shaped two-dimensional covalent organic frameworks reveal crystallographic alignment and fast Li-ion conductivity, Journal of the American Chemical Society, 9767-9770, 138(2016)
158. Chen H, Tu H, Hu C, Liu Y, Dong D, Sun Y, Dai Y, Wang S, Qian H, Lin Z, Cationic covalent organic framework nanosheets for fast Li-ion conduction, Journal of the American Chemical Society, 896-899, 140(2018)
159. Gal N, Lechtman-Goldstein D, Weihs D, Particle tracking in living cells: a review of the mean square displacement method and beyond, Rheologica Acta, 425-443, 52(2013)
160. Wang Y, Richards WD, Ong SP, Miara LJ, Kim JC, Mo Y, Ceder G, Design principles for solid-state lithium superionic conductors, Nature materials, 1026-1031, 14(2015)
161. Zhang K, Zhang B, Weng M, Zheng J, Li S, Pan F, Lithium ion diffusion mechanism in covalent organic framework based solid state electrolyte, Physical Chemistry Chemical Physics, 9883-9888, 21(2019)
162. Jeong K, Park S, Jung GY, Kim SH, Lee Y-H, Kwak SK, Lee S-Y, Solvent-Free, Single Lithium-Ion Conducting Covalent Organic Frameworks, Journal of the American Chemical Society, 5880-5885, 141(2019)
163. Hu Y, Dunlap N, Wan S, Lu S, Huang S, Sellinger I, Ortiz M, Jin Y, Lee S-h, Zhang W, Crystalline lithium imidazolate covalent organic frameworks with high Li-ion conductivity, Journal of the American Chemical Society, 7518-7525, 141(2019)